5.5 W continuous-wave TEM$_{00}$-mode Nd:YAG solar laser by a light-guide/2V-shaped pump cavity

J. Almeida[1] · D. Liang[1] · C. R. Vistas[1] · R. Bouadjemine[1] · E. Guillot[2]

Abstract A significant progress in TEM$_{00}$-mode solar laser power and efficiency with heliostat–parabolic mirror system is reported here. A double-stage light-guide/2V-shaped pump cavity is used to efficiently couple and redistribute the concentrated pump light from a 2-m-diameter parabolic mirror to a 4-mm-diameter, 30-mm-length, 1.1 at.% Nd:YAG single-crystal rod. The light guide with large rectangular cross section enables a stable uniform pumping profile along the laser rod, resulting also in an enhanced tracking error compensation capacity. 5.5 W cw TEM$_{00}$-mode solar laser power was measured at the output of a thermally near unstable asymmetric resonator. 150 and 157 % improvement in TEM$_{00}$-mode solar laser collection efficiency and slope efficiency were obtained, respectively.

1 Introduction

The idea of directly converting incoherent and broadband solar radiation into coherent and narrowband laser radiation has emerged shortly after the invention of laser [1]. Compared to electrically powered lasers, solar-pumped lasers benefit from simplicity and reliability because of the complete elimination of the electrical power generation and

conditioning equipments. Thus, solar lasers offer the prospect of a drastic reduction in the cost of coherent optical radiation for high-average-power applications, leading to numerous environmental and economical advantages. As solar energy is the main continuous energy source in space, this technology becomes particularly attractive for space-based applications [2, 3], where extended run times are required and where compactness, reliability, and efficiency are critical. Solar laser has also large potentials for terrestrial applications such as high-temperature material processing and magnesium–hydrogen energy cycle [4].

Since the first report of "A sun-pumped cw one-watt laser" in 1966 [1], optical and laser material advances have continued to improve solar laser performance. Parabolic mirrors have long been explored to achieve tight focusing of incoming solar radiation [5–9]. Nevertheless, significant progresses in solar laser efficiency have been made in the last decade after the adoption of Fresnel lenses as primary solar concentrators [10–13]. Record-high collection efficiency—defined by the ratio between laser output power and primary concentrator area [8]—of 30.0 W/m^2 was attained by pumping a large Nd:YAG rod through a large Fresnel lens [13]. However, very large $M_x^2 = M_y^2 = 137$ factors have been associated with this approach, resulting in very poor beam quality.

Even thought Fresnel lenses have been preferred due to its simplicity, easy availability, and low cost, there still exist many practical inconveniences, regarding to their use in solar-pumped lasers. A laser head pumped by a typical Fresnel lens solar collection and concentration system moves together with the whole solar tracking structure [10–14]; an optical fiber thus becomes necessary for the transportation of solar laser radiation to a fixed target position. This in turn affects negatively the efficiency of the whole solar laser system due to optical fiber transmission loss.

R. Bouadjemine is on leave from Division of Ionized Gases and Lasers, Centre for Development of Advanced Technology CDTA BP, Baba Hassan, Algiers, Algeria, 16000.

✉ D. Liang
  dl@fct.unl.pt

[1] CEFITEC, Departamento de Física, FCT, Universidade Nova de Lisboa, Campus de Caparica, 2829-516 Lisbon, Portugal

[2] PROMES-CNRS, 7 rue du Four Solaire, 66120 Font Romeu, Odeillo, France

Moreover, Fresnel lenses cause the dispersion of the solar radiation spectrum along its focal zone, hampering the efficient light concentration into a thin laser rod. Minimizing a laser rod volume reduces cost, and reducing the diameter makes the rod more resistant to thermal stress [9]. Also, as the rod acts as an aperture, by pumping a small diameter laser rod, high-order resonator modes can be suppressed by large diffraction losses, and beam quality improves. For these reasons, we have insisted in enhancing the solar laser performance by pumping small diameter Nd:YAG rods through heliostat–parabolic mirror system [15, 16]. Despite the small overlap between the Nd:YAG absorption spectrum and the solar emission spectrum [17], Nd:YAG has been demonstrated as the best material under highly intense solar pumping [5–9, 12–16] because of its excellent characteristic on thermal conductivity ($K = 14$ W/m K [18]), high quantum efficiency and fracture strength ($\sigma_{max} = 180$–210 N/mm^2 [18]). Recently, 4.4 W cw TEM$_{00}$-mode solar laser power was obtained by side-pumping a 3-mm-diameter, 30-mm-length Nd:YAG rod through a heliostat–parabolic mirror system in PROMES-CNRS (Procedes, Materiaux et Energie Solaire-Centre National de la Recherche Scientific). Slope efficiency of 0.81 % and collection efficiency of 1.91 W/m^2 were registered [16]. Many applications of solid-state lasers require operation of the laser at the TEM$_{00}$-mode since it produces the smallest beam divergence, the highest power density and, hence, the highest brightness [18]. Therefore, it is highly desirable to improve the present TEM$_{00}$-mode solar laser efficiency.

Thermal-induced aberrations are limiting factors for generating high-power and high-beam-quality solid-state lasers [19–22]. Thus, to scale our TEM$_{00}$ solar laser to high-average power, a homogeneously pumped laser rod is of utmost importance. The adoption of side-pumping configuration employing rectangular light guides allows a significant reduction in the associated thermal lensing and thermal stress problems as they give uniform absorption distribution along the rod axis [15, 16]. The highly concentrated solar radiation from the primary parabolic concentrator is efficiently transmitted and uniformly redistributed along the 4-mm-diameter, 30-mm-length, 1.1 at.% Nd:YAG rod through the light guide with large rectangular cross section and, thus, high tracking error compensation capacity. The light guide output section has a 2D-trapezoidal shape and is immersed in the water-flooded 2V-shaped pump cavity, enabling the efficient coupling of pump light to the laser rod. Optimum pumping conditions and solar laser beam parameters were found through ZEMAX and LASer Cavity Analysis and Design (LASCAD) numerical analysis. The final test of the solar laser output performance was carried out at PROMES-CNRS during the period of July 2015. For efficient extraction of laser power in fundamental mode, an asymmetric laser resonator was adopted.

5.5 W continuous-wave (cw) TEM$_{00}$-mode ($M^2 \leq 1.25$) solar laser power was measured, being 1.24 times than the previous result with same solar facility. 150 and 157 % improvement in collection efficiency and slope efficiency over the previous record were obtained, respectively [16].

2 Solar-pumped Nd:YAG laser system

### 2.1 Solar energy collection and concentration by the PROMES-CNRS heliostat–parabolic mirror system

A large plane mirror with 36 small flat segments (0.5 m × 0.5 m each), mounted on a two-axis heliostat, redirects the incoming solar radiation toward the horizontal axis primary parabolic mirror with 2 m diameter, 60° rim angle and 850 mm focal length, as shown in Fig. 1a. All the mirrors are back-surface silver-coated. Due to iron impurities within the glass substrates of plane and parabolic mirrors (with 5 and 10 mm thickness, respectively), along with more than 70-year usage, only 59 % of incoming solar radiation is effectively focused to the focal zone. Two sliding doors and a shutter with motorized blades regulate the incoming solar power from the heliostat. After considering all the shading effects in the primary concentrator (the space between the heliostat mirrors, shutter blades, the X–Y–Z axis positioning system, the laser resonant cavity and its mechanical fixation), an effective collection area of 2.65 m^2 was calculated when the shutter was totally opened. On high solar insolation days, more than 1400 W solar power can be focused into a near-Gaussian light spot with 11-mm full width at half maximum (FWHM).

The laser head, composed by the rectangular fused-silica light guide, the 2V-shaped pump cavity and the Nd:YAG rod, is mechanically mounted to the laser resonant cavity, which is fixed on an X–Y–Z axis positioning system by using a multi-angle vice, as shown in Fig. 1b, c. An accurate optical alignment in the focal zone is hence ensured. The Nd:YAG rod was actively cooled by water at 6 L/min flow rate.

2.2 Rectangular fused-silica light guide with high tracking error compensation capacity

The concentrated solar radiation is firstly collected by the rectangular fused-silica light guide with 14 mm × 22 mm input end. It is then transmitted along 70 mm length, through total internal reflection, to its 2D-trapezoidal output section with 9 mm × 22 mm output end and 8 mm length, as illustrated in Fig. 2.

Fused silica is an ideal optical material for Nd:YAG laser pumping since it is transparent over the Nd:YAG absorption spectrum. It has a low coefficient of thermal expansion, and it is resistant to scratching and thermal
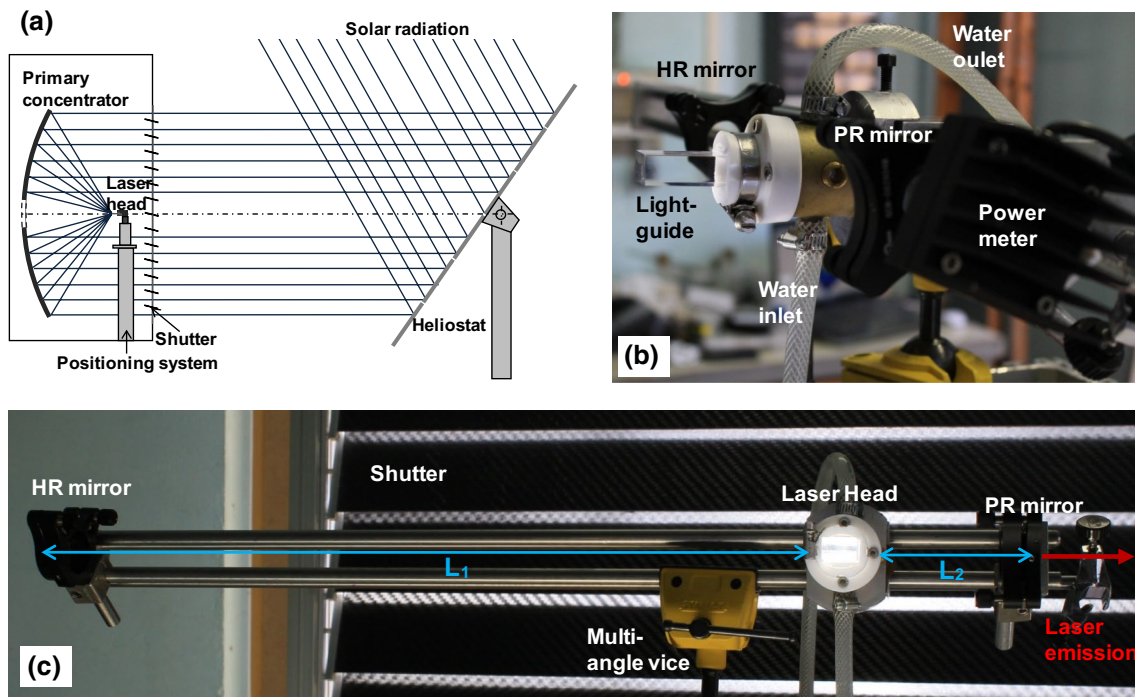
Fig. 1 a Scheme of the PROMES-CNRS heliostat–parabolic mirror system. **b** Solar-pumped Nd:YAG laser system. **c** Front view of the asymmetric laser resonant cavity for extraction of TEM$_{00}$-mode laser. L_1 and L_2 represent the separation length of the high-reflection (HR) and partial-reflection (PR) mirrors to their nearest end face of the laser rod
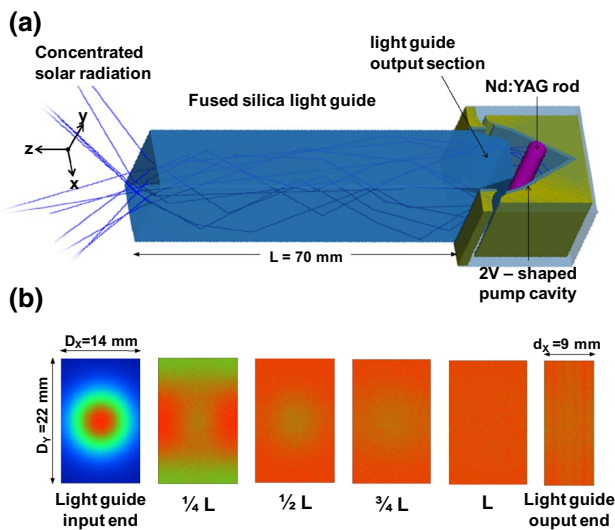

Fig. 2 a 3D design of the solar laser head, composed of the rectangular light guide, the *2V*-shaped pump cavity and the 4-mm-diameter, 30-mm-length 1.1 at.% Nd:YAG rod. **b** Pump light distribution at different sections along the light guide. Uniform pump light distribution is achieved at $L = 70$ mm

shock. To manufacture the light guide, a fused-silica rod of 99.999 % optical purity (supplied by Beijing Aomolin Ltd), with 22 mm diameter and 80 mm length, was ground and polished to its final dimensions.

Heliostat orientation errors usually move the center of the absorption distribution within the laser rod, resulting in less laser output power and a non-uniform beam profile. The light guide with rectangular cross section is therefore essential to overcoming this problem, serving as a beam homogenizer by transforming the near-Gaussian profile of the concentrated light spot at its input end into a uniform pump light distribution at its output end, as shown in Fig. 2b. By using a light guide with large rectangular cross section, one can attain higher transfer efficiency and smaller tracking error-dependent losses compared to that with smaller cross section [16], but the efficient light coupling to the laser crystal can be affected by the large output end. It is therefore straightforward to use a closed cavity pumping arrangement, formed by the narrower output section of the light guide and the water-flooded 2V-shaped pump cavity, as illustrated in Figs. 2a and 5. The rod diameter is also a key parameter for achieving high transfer efficiency and reducing the tracking error-dependent losses.

For the focal distance of 0.85 m, a typical 0.1° tracking error corresponds to approximately 1.5 mm displacement in both X and Y axes. Figures 3 and 4 show the comparison of the influence of the combined tracking error displacement on the absorbed pump flux distributions of the Nd:YAG single-crystal rods pumped through the present pumping scheme and the previous solar laser side-pumping

Fig. 3 Numerical absorbed pump flux distributions along the central and longitudinal cross sections of the 4-mm-diameter, 30-mm-length, 1.1 at.% Nd:YAG rod pumped through the present scheme **a** with no tracking error and **b** considering 0.1° combined tracking error in X, Y axes
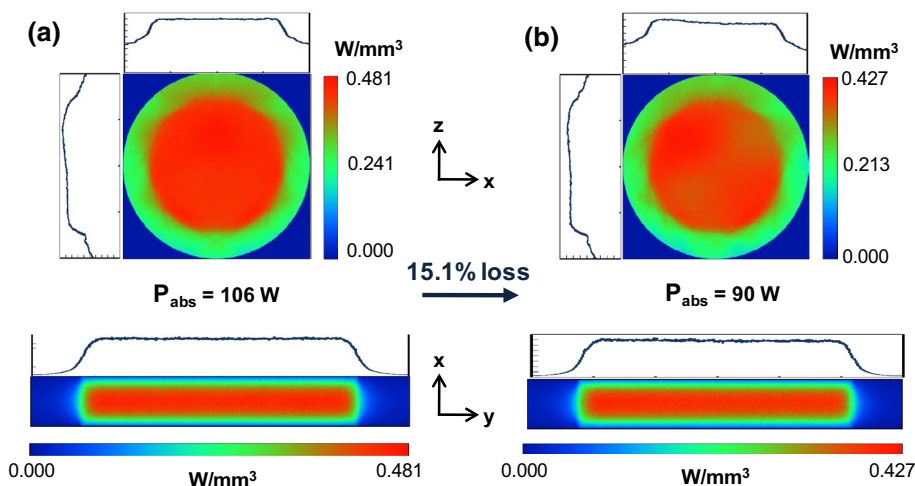
Fig. 4 Numerical absorbed pump flux distributions along the central and longitudinal cross sections of the 3-mm-diameter, 30-mm-length, 1.1 at.% Nd:YAG rod pumped through the previous scheme [16] **a** with no tracking error and **b** considering 0.1° combined tracking error in X, Y axes
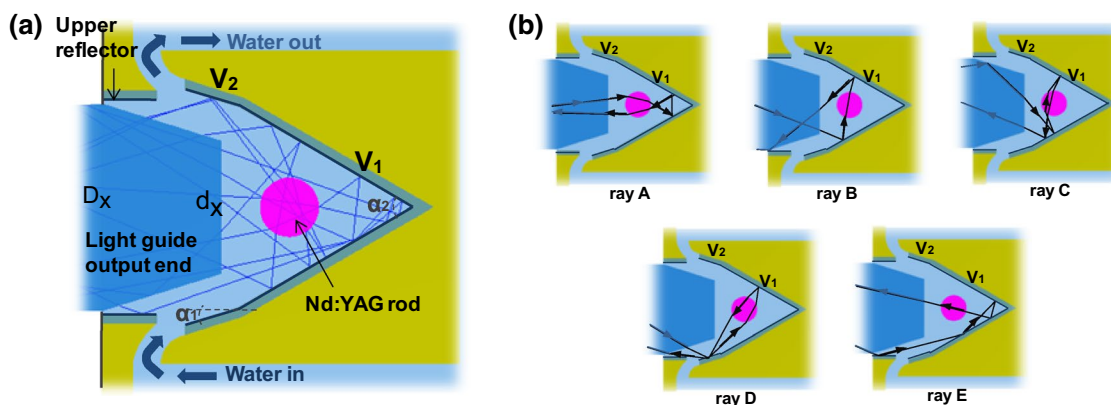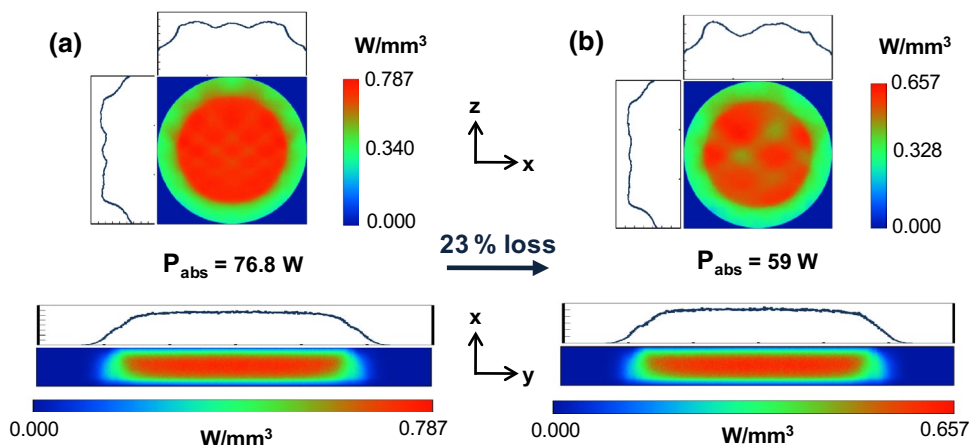
Fig. 5 **a** The 2V-shaped pump cavity, within which the 4-mm-diameter Nd:YAG rod is efficiently pumped due to multi-pass absorption of pump radiation. **b** Examples of the passage of the pump rays with different incidence angles within the 2V cavity

approach [16], respectively. In the latter, a light guide with smaller rectangular cross section, a 2D-CPC concentrator and a V-shaped reflector were combined to pump a 3-mm-diameter, 30-mm-length laser rod.

As shown in both Figs. 3 and 4, the focal spot shift along Y axis results only in a uniform reduction in the pump flux along both rod axes. The focal spot shift along X axis, however, moves the center of the absorbed pump profile along the

central cross section of the rod. This displacement is more pronounced in the 3-mm-diameter Nd:YAG rod, pumped through the previous scheme, resulting in increased loss of absorbed pump power compared to the 4-mm-diameter Nd:YAG rod pumped through the present pumping scheme.

2.3 The 2V-shaped pump cavity

The two-dimensional 2V-shaped cavity (Fig. 5) has an entrance aperture of 16 mm × 22 mm and 15.3 mm depth. It is composed of a V-shaped reflector V_1, with $\alpha_1 = 60°$ opening angle, and two upper planar reflectors V_2, making an inclination of $\alpha_2 = 17.5°$ in relation to V_1. This 2V combination is much more efficient in coupling the pump rays, with different incidence angles from the light guide to the laser rod, as compared to a single V-shaped reflector. As shown in Fig. 5b, ray A passes through the rod once and is bounced back by V_1, so that double-pass absorption is accomplished. The rays that do not hit directly the laser rod can be redirected by either V_1, making one passage (ray B) or two passages (ray C) through the laser rod, or V_2 (ray D). The upper reflectors play also an important role in redirecting the rays (ray E) that exit the inclined faces of the water-flooded light-guide output section toward the 2V cavity, so that at least one passage through the laser rod is accomplished. The inner walls of both V_1, V_2 and upper reflectors are bonded with a protected silver-coated aluminum foil with 94 % reflectivity. Water material also ensures an efficient light coupling, while partially preventing both UV solarization and IR heating to the laser rod.

By combining the pumping features of the 2V-shaped pump cavity with the homogenization capacity of the rectangular light guide, uniform pump power deposition within the laser rod is achieved, as already shown in Fig. 3. For low-average-power operation, in which thermal lensing is moderate, the overlap of the laser mode with an excitation peaked at the center of the rod can be advantageous. However, at high-average output power, when the absorption profile is centrally peaked, the temperature on the axis increases further, resulting in stronger thermal lensing at the center, higher-order aberrations at the periphery and larger stress in the laser rod compared with those of uniform excitation [23]. Consequently, to scale our solar-pumped rod laser to high TEM$_{00}$-mode average power, it is of utmost importance for us to start with a uniform pump power deposition within the laser rod.

3 Numerical optimization of the solar laser design parameters

Similar to our previous solar pumping approaches [12, 14–16], all the above-mentioned design parameters of the

solar laser system are firstly optimized by non-sequential ray-tracing (ZEMAX) software for achieving the maximum absorbed pump power and suitable pump profile within the laser rod. For 1.1 at.% Nd^{3+}-doped YAG single-crystal medium, 22 absorption peaks are defined in ZEMAX numerical data. All the peak wavelengths and their respective absorption coefficients are added to the glass catalogue in ZEMAX software. Solar irradiance values for the above-mentioned 22 peak absorption wavelengths could be consulted from the standard solar spectra for AM1.5 [24] and saved as source wavelength data. During ray tracing, the active medium is divided into a total of 18,000 zones. The path length in each zone is found. With this value and the effective absorption coefficient, the absorbed power within the laser medium can be calculated by summing up the absorbed pump radiation of all zones.

Figure 6 shows the influence of the width D_X of the light guide on the absorbed pump power in the rod. Maximum absorbed pump power of 106 W is numerically achieved with $D_X = 14$ mm light guide. Optimized output aperture $d_X = 9$ mm is also found in this case.

The absorbed pump flux data from the ZEMAX analysis is processed by LASCAD software to study the laser beam parameters and quantify the thermal effects applied in the active medium. The stimulated emission cross section of 2.8×10^{-19} cm^{-1}, the fluorescence lifetime of 230 μs [18] and a typical absorption and scattering loss of 0.003 cm^{-1} for the 1.1 at.% Nd:YAG medium are adopted in LASCAD analysis. An averaged solar pump wavelength of 660 nm is also considered in the analysis [5]. The optical resonator is comprised of two opposing parallel mirrors at right angles to the axis of the active medium, as shown in Fig. 7. One end mirror is high reflection (HR, 99.98 %) coated. The output coupler is partial reflection (PR) coated. The amount of feedback is determined by the reflectivity of the PR mirror.
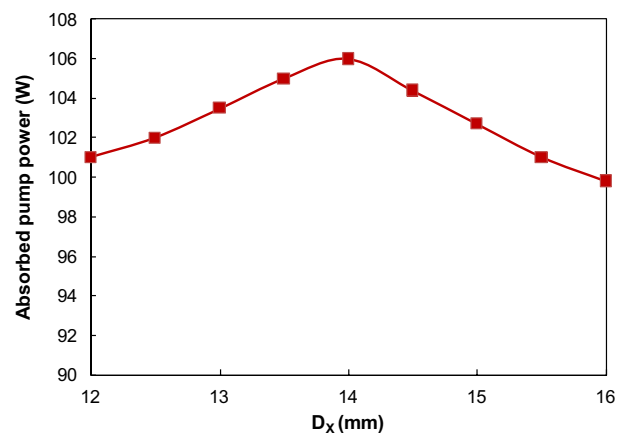
**Fig. 6** Numerically calculated absorbed pump power as function of the light-guide width D_X

Fig. 7 Schematic diagram of the TEM$_{00}$-mode beam propagation along the asymmetric laser resonator with large RoC (radius of curvature) end mirrors, obtained through LASCAD analysis
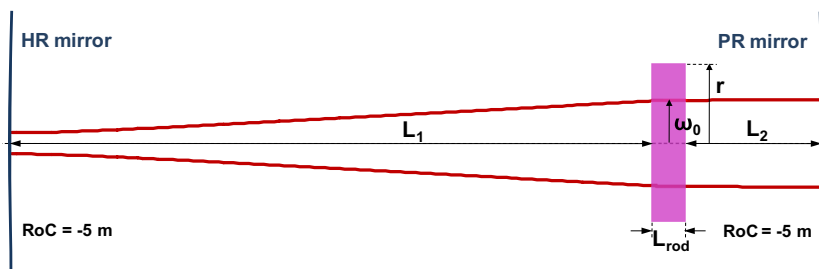
L_1 and L_2 represent the separation length of the HR and PR mirrors to their nearest end face of the laser rod, respectively.

Conventionally, lasers are designed to operate at the middle of thermally stable zones, where the fundamental mode size is insensitive to thermal perturbation [22]. To filter higher-order modes, one classically inserts a pinhole inside the laser cavity. The pinhole diameter roughly matches the fundamental mode size, to prevent the larger higher-order mode from oscillating [21]. However, when the fundamental mode diameter is much smaller than the size of the gain region, the pinhole dramatically reduces the laser extraction efficiency due to poor utilization of the stored energy in the active medium. A suitable resonator design for efficient energy conversion to the TEM$_{00}$-mode must maximize the overlap integral of the resonator TEM$_{00}$-mode and the pump profile while simultaneously utilizing the rod to apodize higher-order spatial modes [25]. The adoption of the asymmetric resonator configuration with concave end mirrors of large radius of curvature (RoC), as illustrated in Fig. 7, has shown to provide a large spatial overlap between the fundamental mode and pump mode volumes [14, 16]. L_1 is a key parameter for achieving the optimum mode overlap. As shown in Fig. 8, as L_1 increases, the fundamental mode size grows up, especially for higher input powers. Thus, if we aim to obtain efficient extraction of TEM$_{00}$-mode laser, the laser should operate close to the edge of the optically stable region, where the fundamental mode size is more sensitive to thermal focus fluctuations. With further increase in pump power, the fundamental mode size would grow up automatically to a value suitable for TEM$_{00}$-mode operation and very good beam quality is expected.

In LASCAD program, the focal length of the rod lens can be determined through the stability limits of a flat–flat resonator. Analogous to the resonator design in Fig. 7, one end mirror is fixed at a close distance to the rod lens, L_2. For a fixed pump power, the focal length of the rod lens is hence given by L_1 at the point in which the resonator becomes unstable. Figure 9a shows the numerically calculated rod focal length as function of the pump power at the focus. The focal length decreases as pump power increases. The numerically calculated values of temperature and heat load in the rod, for the different input powers, are also given in Fig. 9b, c, respectively.
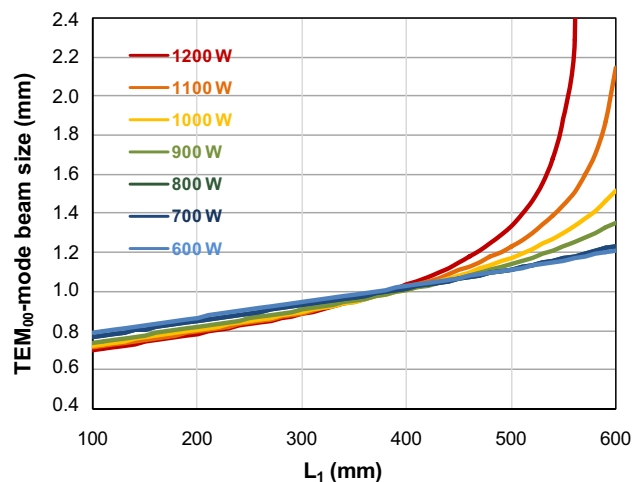

Fig. 8 Numerically obtained TEM$_{00}$-mode beam size within the rod as function of L_1, for different input solar powers at the focus

In LASCAD© analysis, output couplers of different reflectivity (R) were tested to maximize the laser extraction efficiency. Table 1 compares the maximum laser power, slope efficiency and threshold pump power numerically achieved for three different reflectivity output mirrors. A short symmetric laser resonator is adopted in this case. Considering maximum 1450 W pump power at the focus of the 2-m-diameter parabolic mirror, maximum laser power of 21.2 W and slope efficiency of 2.2 % are numerically found for $R = 94$ % output mirror, which agrees well with the experimental measurements in Sect. 4.1. Higher slope efficiency of 2.5 % is numerically predicted for $R = 90$ % output mirror, but only 17 W laser power is achieved. Also, stronger pump power is required to achieve laser emission threshold. $R = 98$ % output mirror offers the lowest threshold pump power, but the slope efficiency is low. For these reasons, $R = 94$ % PR mirror was adopted in our experimental measurements (Sect. "4.1").

4 Solar laser oscillation experiments

Based on the ZEMAX and LASCAD numerically optimized design parameters of the solar laser system, a
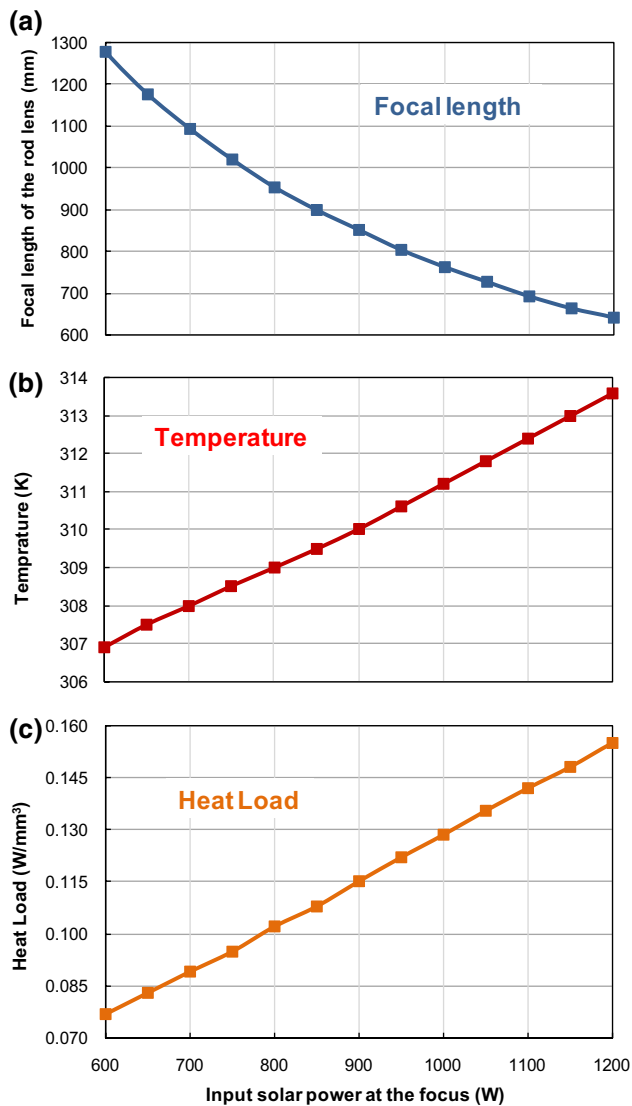
Fig. 9 Numerically calculated **a** rod focal length, **b** temperature and **c** heat load in the rod, for different input solar powers, assuming $T = 300$ K water cooling

Table 1 Solar laser performance for different PR mirror reflectivity

Reflectivity	90 %	94 %	98 %
Maximum laser power	17.2 W	21.2 W	16.8 W
Slope efficiency	2.5 %	2.2 %	1.4 %
Threshold pump power	757 W	502 W	228 W

prototype was built in Lisbon and tested in PROMES-CNRS during July 20–24, 2015. The 4-mm-diameter, 30-mm-length Nd:YAG is supplied by Altechna Co, Ltd. It has 1.1 % Nd^{3+} concentration. Both ends of the rod are anti-reflection (AR)-coated ($R < 0.2$ % @ 1064 nm). The resonator mechanics was designed to allow the
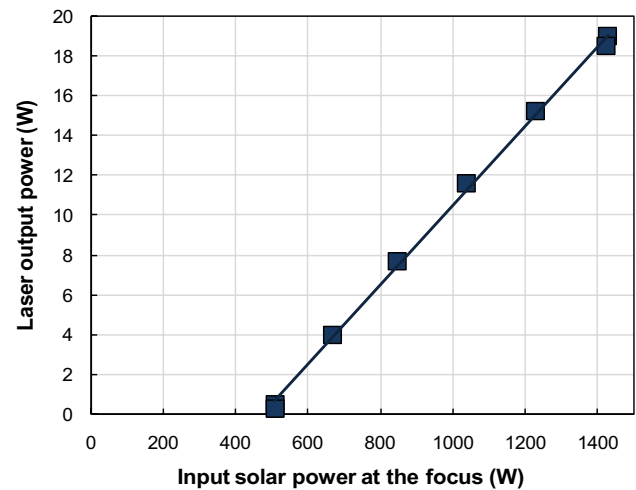
Fig. 10 Nd:YAG multi-mode laser output power versus solar input power at the focus

displacement of the HR mirror (from $L_1 = 120$ mm to $L_1 = 580$ mm), while maintaining the PR mirror at a fixed $L_2 = 120$ mm position. Direct solar irradiance was measured simultaneously during laser experiments with a Kipp & Zonen CH1 pyrheliometer on a Kipp & Zonen 2AP solar tracker. It varied between 810 and 995 W/m^2 during the experiments.

4.1 Multimode solar laser operation

For multimode operation, a symmetric resonator is adopted, with $L_1 = L_2 = 120$ mm. An output coupler with 94 % reflectivity and RoC $= -1$ m is used to achieve maximum extraction of laser output power. By varying the rotation angle of the shutter, different input solar powers and output laser powers were respectively measured with a Molectron PowerMax 500D and a Thorlabs PM1100D power meters. For 2.65 m^2 effective collection area (with the shutter totally opened) and 914 W/m^2 solar irradiance, 1430 W was measured at the focus of the primary concentrator. Maximum laser power of 19 W was measured in this case. A linear slope efficiency of 2.1 % was experimentally achieved, as shown in Fig. 10.

4.2 Fundamental mode solar laser operation

For TEM$_{00}$-mode operation, the HR mirror is shifted to $L_1 = 580$ mm. A 94 % reflectivity output coupler with large RoC $= -5$ m was used in this case. Figure 11 shows the laser output power as function of the input solar power at the focus.

Laser starts to oscillate at an input power of 570 W approximately and grows almost linearly until the pump
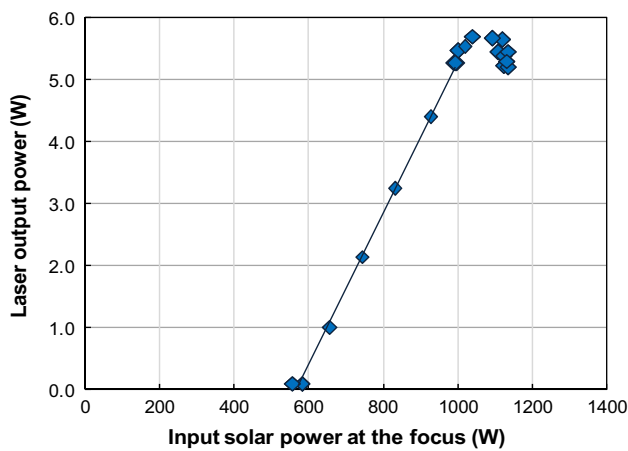
Fig. 11 Laser output power (at $L_1 = 580$ mm) as function of the solar input power at the focus

power reaches about 1000 W. With further increase in pump power, laser output power approaches to a peak value and then drops abruptly, meaning that the resonator has moved out of stability zone. Compared with the increment of rod gain, which is proportional to the pump power, the diffraction loss, that is caused by thermally induced aberration, increases more rapidly as the pump power increases, and consequently, the laser output power is limited. The small concave curve at higher input powers possibly results from birefringence [22]. 1.27 % slope efficiency is experimentally measured, representing an improvement of 157 % over that of the previous TEM$_{00}$-mode solar laser.

A CINOGY UV-NIR beam profiler, CinCam CMOS was used for monitoring the laser beam profile during the experiments. Figure 12a–d shows the evolution of the laser beam profile with pump powers higher than 1000 W.

Since no aperture is used in the laser resonator besides the rod itself, oscillation of higher-order modes occurs at low output powers due to the relatively small overlap between the fundamental mode volume and the pumped region. With the increase in pump power, and thus diffraction loss, only few modes become possible to oscillate, as

shown in Fig. 12a. While pump power is going near thermal stability limit, the resonator modes give rise to only one mode of higher intensity, in Fig. 12d. 5.5 W TEM$_{00}$-mode laser power was registered in this case, for an effective collection area of 1.92 m^2 (with the shutter opened at 80 %), corresponding to 2.84 W/m^2 TEM$_{00}$-mode solar laser collection efficiency. This value is 1.5 times higher than the previous result [16]. The slight discrepancy in laser beam diameters at $1/e^2$ along X and Y axes (Fig. 12e) can be justified by the slight pump profile misalignment due to heliostat orientation error.

Laser beam quality factors were determined by measuring the beam diameter at $1/e^2$ in a near-field position (40 mm from the output coupler) and a far-field position (3 m away from the output coupler). The laser beam divergence θ was found by using Eq. (1)

$$\tan \theta = (\phi_2 - \phi_1)/2L \tag{1}$$

where ϕ_1 and ϕ_2 are the measured laser beam diameters at $1/e^2$ width, 40 mm and 3 m away from the output mirror, respectively, and L is the distance between these two points. M^2 factor was then calculated by Eq. (2)

$$M^2 = \theta/\theta_0 \tag{2}$$

where $\theta_0 = \lambda/\pi\omega_0$ is the divergence of diffraction-limited Gaussian beam for $\lambda = 1.064$ μm and $\omega_0 = 1170$ μm, as calculated by LASCAD laser beam propagation method for the 4-mm-diameter, 30-mm-length, 1.1 at.% Nd:YAG rod.

Due to the heliostat orientation errors during solar laser operation, its M^2 factors measurement has become a challenging task, since solar lasers do not benefit from the same stable optical pumping conditions of electrically pumped lasers. Therefore, solar laser M^2 factor measurements from standard methods, which usually take many minutes to accomplish, can also lead to poor measurement accuracy due to the slight shifts of the focal spot in relation to the input face of the light guide. This is even more significant if the solar laser works near the stability limit of the asymmetric laser resonator. For these reasons, our laser beam quality factors were determined by the quick measurement of

Fig. 12 a–d Evolution of output laser beam profile (taken 1.7 m away from the output coupler) with pump power as it approaches the resonator stability limit. **e** 2D analysis of the measured TEM$_{00}$-mode profile
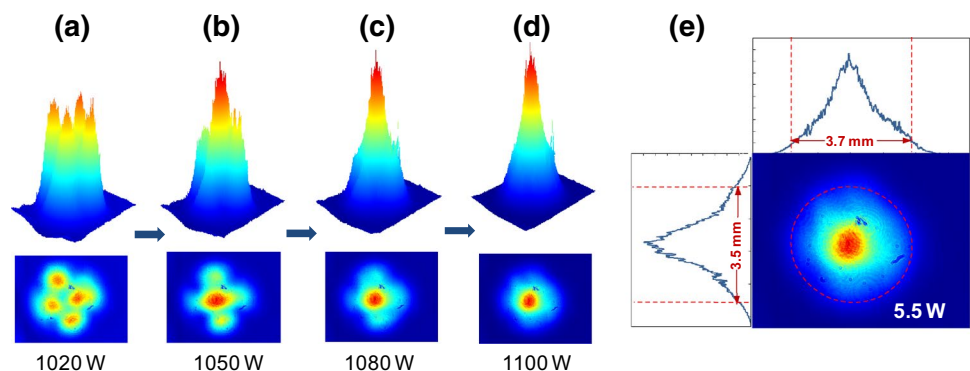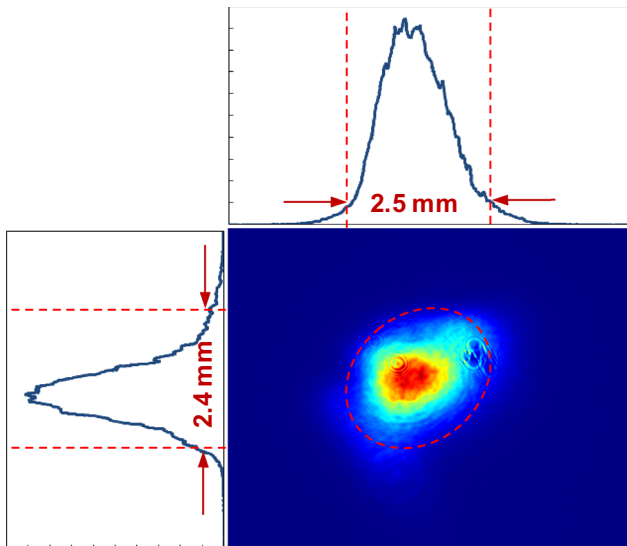
Fig. 13 Measured near-field TEM_{00}-mode laser beam pattern

laser beam diameter at $1/e^2$ at both near-field and far-field positions. The thermal lens effect on the laser beam propagation was also taken into account in LASCAD analysis, as mentioned in Sect. 3. The value of the TEM_{00}-mode beam waist size can be obtained by measuring the laser beam diameter at $1/e^2$ width ϕ_1 at near-field position. Figure 13 shows the near-field TEM_{00}-mode laser beam profile (taken 40 mm away from the output coupler). Average TEM_{00}-mode beam diameter $\phi_1 = 2.45$ mm was measured, as shown in Fig. 13, which agreed well with the numerically calculated value in LASCAD analysis at the same position. $M_x^2 \approx 125$ and $M_y^2 \approx 1.14$ factors were finally determined. Considering the heliostat orientation error during laser emission, $M_x^2 \approx M_y^2 \leq 1.25$ are considered as adequate values for describing the laser beam quality.

5 Conclusions

The adoption of the side-pumping configuration by employing the fused-silica light guide with large rectangular cross section enables a stable uniform pumping profile. The efficient light coupling to the laser rod is ensured by the closed-coupled pumping arrangement formed by the water-flooded 2D-trapezoidal output section of the light guide and the 2V cavity, which allows multi-pass absorption of pump radiation. The present solar laser pumping approach allows higher tracking error compensation capacity compared to the previous one with same solar facility. By adopting a short symmetric laser resonator, multimode solar laser power of 19 W was measured. 2.1 % slope efficiency was obtained. For

the efficient extraction of TEM_{00}-mode solar laser, a long asymmetric laser resonator was used instead, since it offers a good overlap between the fundamental mode and the pumped region of the active medium. 5.5 W cw TEM_{00}-mode solar laser ($M^2 \leq 1.25$) was registered. 2.84 W/m^2 collection efficiency and 1.27 % slope efficiency were found, representing an enhancement of 150 and 157 %, respectively, over that of the previous TEM_{00}-mode solar laser.

References

1. C.G. Young, Appl. Opt. **5**, 993 (1966)
2. J.D.G. Rather, E.T. Gerry, G.W. Zeiders, NASA Technical Reports Server (NTRS), May 25 (1977)
3. Space Solar Power Limitless clean energy from space, National Space Society, March 26 (2013)
4. T. Yabe, S. Uchida, K. Ikuta, K. Yoshida, C. Baasandash, M.S. Mohamed, Y. Sakurai, Y. Ogata, M. Tuji, Y. Mori, Y. Satoh, Y. Ohkubo, M. Murahara, A. Ikesue, M. Nakatsuka, T. Saiki, S. Motokoshi, C. Yamanaka, Appl. Phys. Lett. **89**, 261107 (2006)
5. M. Weksler, J. Shwartz, IEEE J. Quantum Electron. **24**, 1222 (1988)
6. H. Arashi, Y. Oka, N. Sasahara, A. Kaimai, M. Ishigame, Jpn. J. Appl. Phys. **23**, 1051 (1984)
7. R.M.J. Benmair, J. Kagan, Y. Kalisky, Y. Noter, M. Oron, Y. Shimony, A. Yogev, Opt. Lett. **15**, 36 (1990)
8. M. Lando, D.G. Jenkins, H. Bernstein, J.J. O'Gallagher, R. Winston, A. Lewandowski, Proc. SPIE **2426**, 478 (1995)
9. M. Lando, J. Kagan, B. Linyekin, V. Dobrusin, Opt. Commun. **222**, 371 (2003)
10. T. Yabe, T. Ohkubo, S. Uchida, M. Nakatsuka, T. Funatsu, A. Mabuti, A. Oyama, Y. Nakagawa, T. Oishi, K. Daito, B. Behgol, Y. Nakayama, M. Yoshida, S. Motokoshi, Y. Sato, C. Baasandash, Appl. Phys. Lett. **90**, 261120 (2007)
11. T. Ohkubo, T. Yabe, K. Yoshida, S. Uchida, T. Funatsu, B. Bagheri, T. Oishi, K. Daito, M. Ishioka, Y. Nakayama, N. Yasunaga, K. Kido, Y. Sato, C. Baasandash, K. Kato, T. Yanagitani, Y. Okamoto, Opt. Lett. **34**, 175 (2009)
12. D. Liang, J. Almeida, Opt. Express **19**, 26399 (2011)
13. T.H. Dinh, T. Ohkubo, T. Yabe, H. Kuboyama, Opt. Lett. **37**, 2670 (2012)
14. D. Liang, J. Almeida, Opt. Express **21**, 25107 (2013)
15. J. Almeida, D. Liang, E. Guillot, Opt. Laser Technol. **44**, 2115 (2012)
16. D. Liang, J. Almeida, C.R. Vistas, E. Guillot, Sol. Energy Mat. Sol. Cells **134**, 305 (2015)
17. B. Zhao, C. Zhao, J. He, S. Yang, Acta Opt. Sin. **2007**, 1 (2006)
18. W. Koechner, *Solid-state laser engineering* (Springer, Berlin, 1999)

19. Y. Hirano, Y. Koyata, S. Yamamoto, K. Kasahara, T. Tajime, Opt. Lett. **24**, 679 (1999)
20. W. Xie, S.C. Tam, Y.L. Lam, J. Liu, H. Yang, J. Gu, W. Tan, Appl. Opt. **39**, 5482 (2000)
21. J. Bourderionnet, A. Brignon, J.P. Huignard, R. Frey, Opt. Commun. **204**, 299 (2002)
22. Y. Feng, Y. Bi, Z. Xu, SPIE **4969**, 227 (2003)
23. T. Brand, Opt. Lett. **20**, 1776 (1995)
24. ASTM Standard G173 - 03 (2012)
25. D. Welford, D.M. Rines, B.J. Dinerman, Opt. Lett. **16**, 1850 (1991)